JOURNAL OF GEOPHYSICAL RESEARCH: SOLID EARTH, VOL. 118, 2347–2355, doi:10.1002/jgrb.50202, 2013

Spatio-temporal variations of double-couple aftershock mechanisms and possible volumetric earthquake strain

Z. E. Ross[1] and Y. Ben-Zion[1]

Received 25 December 2012; revised 19 April 2013; accepted 24 April 2013; published 28 May 2013.

[1] We analyze spatio-temporal patterns in rotation angles of double-couple–constrained mechanisms of aftershocks of the 1992 Landers earthquake. The rotation angles provide information on the distribution of source geometries in different regions of space and time with respect to the mainshock focal mechanism. The results indicate that the mechanisms of the early aftershocks are more scattered and less aligned with the mainshock than those of the long-term events. This is most pronounced around the northern end of the Landers rupture, least pronounced around the central section, and intermediate around the southern end of the rupture. The relatively large scatter and misalignment of the mean rotation angles of the early focal mechanisms around the edges of the Landers rupture suggest possible volumetric earthquake strain in these regions. The results may reflect isotropic source terms produced by dynamic generation of rock damage. Synthetic tests indicate that the observed differences in the rotation distributions of the early and long-term events around the end regions of the Landers rupture can result from neglecting in the inversion process isotropic components that are 0.03–0.15 of the total event moments.

Citation: Ross, Z. E., and Y. Ben-Zion (2013), Spatio-temporal variations of double-couple aftershock mechanisms and possible volumetric earthquake strain, *J. Geophys. Res. Solid Earth*, *118*, 2347–2355, doi:10.1002/jgrb.50202.

1. Introduction

[2] Most studies on the physics and properties of crustal earthquakes focus on deviatoric/shear stress-strain components. This holds for routine derivations of earthquake source parameters, laboratory experiments, and simulations of earthquake and fault dynamics over both short and long time scales. While the changes of stress and strain during crustal earthquakes are predominantly deviatoric [e.g., *Reid*, 1910; *Riedesel and Jordan*, 1989; *Dufumier and Rivera*, 1997], even small dynamic variations of volumetric and normal stress-strain components can have fundamental implications for many aspects of earthquake and fault mechanics. For example, the evolution of fault resistance to motion with slip, and more generally the energy partitioning during faulting, can be altered dramatically by changes of normal stress and volumetric deformation. Transient changes of normal stress may be produced within earthquake rupture zones by mechanisms ranging from sliding on rough surfaces, ruptures on bimaterial interfaces and various fluid-thermal effects [e.g., *Brune et al.*, 1993; *Ben-Zion*, 2001; *Rice*, 2006]. Dynamic changes of elastic moduli in earthquake source volumes can generate damage-related radiation associated with a significant isotropic component [*Ben-Zion and Ampuero*, 2009]. This is expected especially near rupture ends, geometrically complex fault sections and regions without large preexisting faults. Recent observations of enhanced high-frequency *P* waves from aftershocks of the 2010 El Mayor-Cucapah earthquake may reflect damage-related isotropic radiation from earthquake source volumes [*Castro and Ben-Zion*, 2013].

[3] Individual earthquakes may be viewed as sensors of inelastic strain associated with slip patches of various sizes distributed throughout the seismogenic zone. The potency tensors P_{ij} of earthquakes, computed from catalogs of focal mechanisms, can be used to describe 4-D patterns of seismic strain fields. The degree of heterogeneity of a seismic strain field in a region can be quantified by calculating the distribution of rotations among sets of potency tensors. The stability of results can be increased using summed potency tensors instead of individual ones [e.g., *Bailey et al.*, 2010]. Typical focal mechanism inversions constrain the solutions to be deviatoric [e.g., *Hardebeck and Shearer*, 2002; *Yang et al.*, 2012], so the isotropic components of individual source tensors are by default zero. Nevertheless, populations of derived deviatoric mechanisms can be used to track collectively the 4-D variations of the seismic strain field, including volumetric components, around earthquake rupture zones.

[4] In the present paper, we attempt to find signatures of volumetric components of faulting by analyzing rotations of double-couple–constrained focal mechanisms. To have a high density of events in a geometrically complex area, we examine aftershocks of the 1992 M_w 7.3 Landers earthquake (Figure 1). In regions surrounding the north and south ends

Additional supporting information may be found in the online version of this article.

[1]Department of Earth Sciences, University of Southern California, Los Angeles, California, USA.

Corresponding author: Z. E. Ross, Department of Earth Sciences, University of Southern California, Los Angeles, CA 90089-0740, USA. (zross@usc.edu)

2169-9313/13/10.1002/jgrb.50202

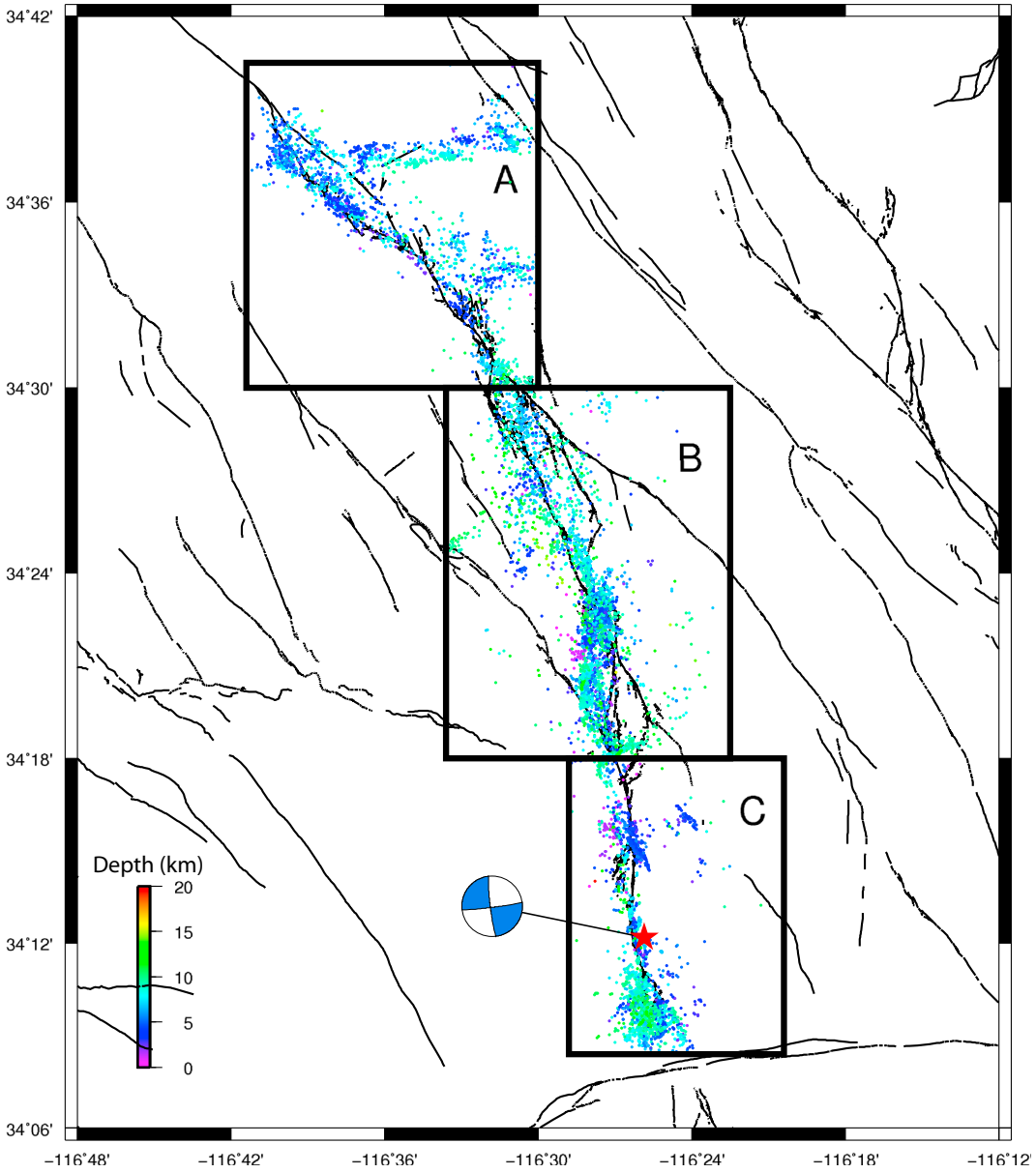

Figure 1. Aftershocks of the 1992 *M* 7.3 Landers earthquake (red star and focal mechanism) in the eastern California shear zone. The study area is divided into three approximately equal regions surrounding the two rupture ends and the central section. The epicenter locations (color-coded by depth), and associated double-couple–constrained mechanisms used in the analysis, are from the regional 1980–2010 focal mechanism catalog of *Yang et al.* [2012].

of the Landers mainshock rupture we find clear deviations in the distribution of rotations of early aftershock mechanism from the long-term pattern. The deviations decay gradually within about a year from the time of the Landers mainshock to the common regional pattern. The results may be explained in terms of small isotropic source components in the early aftershocks near the rupture ends, where they are expected to exist, which were neglected in the derivation of the double-couple (DC) mechanisms.

2. Methodology and Results

[5] We examine spatio-temporal variations in the orientations of aftershock focal mechanisms, constrained to be double-couples, for evidence of isotropic source components. We anticipate the size of the isotropic source component of regular tectonic earthquakes to be generally small, but to increase in areas (e.g., near rupture ends) where the faulting process is expected to produce rock fracturing. To have statistically significant tests, we need a sufficiently large number of events. In this work we analyze aftershocks of the 1992 M_w 7.3 Landers earthquake that was associated with complex faulting and produced a high density of aftershocks in a narrow space-time window. We assume that early aftershocks respond to and largely reflect stress-strain changes produced by the mainshock, and that with increasing time later aftershocks return progressively to a response that reflects the regional background field.

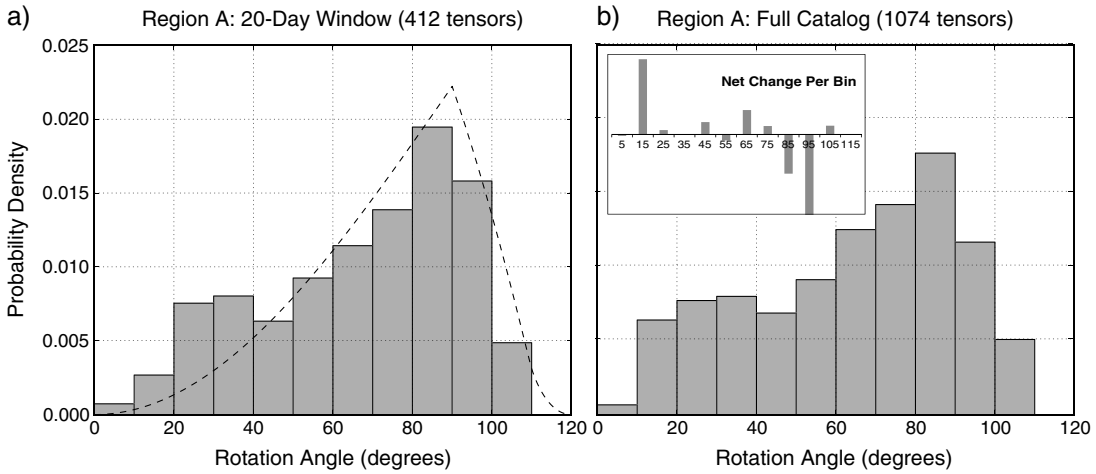

Figure 2. Histograms of rotation angles of the double-couple–constrained mechanisms of aftershocks in the northern region A of Figure 1. The black dashed lines show the analytic probability density function for rotation angles between randomly oriented double couples [*Kagan*, 1992]. (a) Results for events within 20 days of the Landers mainshock. (b) Results for all events in the 1980–2010 catalog. The results show considerable scatter from the orientation of the Landers mainshock mechanism and overall migration of angles from high to low values. The bars in the inset show the net changes of probability density for each bin between Figures 2a and 2b. In Figure 2a there are approximately 9% more the rotation angles above 70° than in Figure 2b and nearly all bins below 70° show a net increase of probability density.

[6] The source of each earthquake is quantified with the seismic potency tensor given by [*Ben-Zion*, 2003]

$$P_{ij} = \int_V \varepsilon_{ij}^{\mathrm{T}} \mathrm{d}V \tag{1}$$

where $\varepsilon_{ij}^{\mathrm{T}}$ is the transformational strain [e.g., *Eshelby*, 1957] and V is the source volume. The potency tensor is a strain-based analog of the seismic moment tensor M_{ij} [*Backus and Mulcahy*, 1976; *Ampuero and Dahlen*, 2005] given by the product of the potency tensor with the tensor of elastic moduli at the source [*Ben-Zion*, 2008; *Chapman and Leaney*, 2012]. We prefer to use potency tensors because they represent the seismic source without making assumptions on values of elastic moduli at the source volumes. The analysis employs the relocated Southern California focal mechanism catalog of *Yang et al.* [2012], constrained to be double-couples and derived with the program HASH using first motion polarities and amplitude ratios [*Hardebeck and Shearer*, 2002]. The seismic potency of each event is obtained from the magnitude using the empirical magnitude-potency scaling relation of *Ben-Zion and Zhu* [2002].

[7] The magnitude of completeness of earthquakes in the Landers area is estimated to be about M 2.2. There are 4139 recorded aftershocks around the Landers rupture with $M \geq 2.2$ (small circles in Figure 1) from the time of the mainshock (28 June 1992) until the end of the employed catalog (31 December 2010). The number of $M \geq 2.2$ aftershocks within 20 days of the mainshock is 1031. To examine aftershock focal mechanism orientations in regions expected to be associated with different amounts of rock fracturing, we divide the study area into three portions. Regions A and C are around the ends of the Landers rupture while region B is around the central section of the rupture zone (Figure 1).

[8] An earthquake source tensor can be defined by the orientations of its principal axes, P, T, and B, and the set of corresponding eigenvalues. To examine signatures of possible evolution or heterogeneity in the orientations of these axes, we need a measure of the difference between two orientation tensors A and B. This is provided by the angle necessary to rotate one set of principal axes into another, which is defined by [*Kagan*, 1991]

$$\Omega = 2 \arccos(q_0) \tag{2}$$

where q_0 is the scalar component of a normalized quaternion $q' = q_0 + q_1 i + q_2 j + q_3 k$ that describes the rotation. The angle of rotation is defined for $0° \leq \Omega \leq 120°$, which means that no two sets of principal axes can be more than 120° apart. There are four different ways of rotating a source tensor to the same final orientation. Here we use the minimum of the four angles, which can be obtained by [*Kuipers*, 2002]

$$\Omega_{\min} = \arccos\left(\frac{\max(Tr(\mathbf{R}_1), Tr(\mathbf{R}_2), Tr(\mathbf{R}_3), Tr(\mathbf{R}_4)) - 1}{2}\right) \tag{3}$$

where

$$\begin{aligned}
\mathbf{R}_1 &= \left(\mathbf{e}_1^A, \mathbf{e}_2^A, \mathbf{e}_3^A\right)\left(\mathbf{e}_1^B, \mathbf{e}_2^B, \mathbf{e}_3^B\right)^{\mathrm{T}} \\
\mathbf{R}_2 &= \left(-\mathbf{e}_1^A, \mathbf{e}_2^A, -\mathbf{e}_3^A\right)\left(\mathbf{e}_1^B, \mathbf{e}_2^B, \mathbf{e}_3^B\right)^{\mathrm{T}} \\
\mathbf{R}_3 &= \left(\mathbf{e}_1^A, -\mathbf{e}_2^A, -\mathbf{e}_3^A\right)\left(\mathbf{e}_1^B, \mathbf{e}_2^B, \mathbf{e}_3^B\right)^{\mathrm{T}} \\
\mathbf{R}_4 &= \left(-\mathbf{e}_1^A, -\mathbf{e}_2^A, \mathbf{e}_3^A\right)\left(\mathbf{e}_1^B, \mathbf{e}_2^B, \mathbf{e}_3^B\right)^{\mathrm{T}}
\end{aligned}$$

with $\mathbf{e}_i^A$ and $\mathbf{e}_i^B$ being the ith eigenvectors of tensors A and B, respectively. Below we denote for simplicity the minimum rotation angle as Ω.

[9] Because the rotation angle does not take into account the eigenvalues of the source tensors, it solely represents their angular misalignment. In the following, we use the

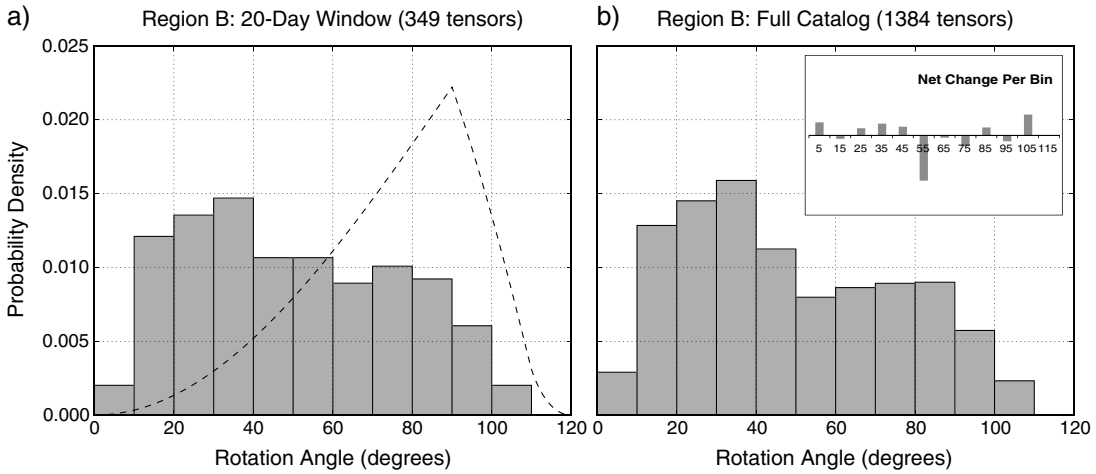

Figure 3. (a–b) Similar to Figure 2 for events in the central region B of Figure 1. The results exhibit considerably less scatter and temporal evolution than in region A, with lack of statistically significant difference between the two populations. The inset in Figure 3b shows that the net changes between Figures 3a and 3b are relatively small compared to those in Figure 2.

mainshock potency tensor to define a reference orientation, and compute the set of minimum rotation angles between the reference and each of the aftershock tensors within given spatio-temporal bounds. The sampling distribution of these angles is an indicator of the heterogeneity of the aftershock focal mechanism orientations, and traditional statistics can be used to describe the aspects of the sample. Using the Landers focal mechanism as a reference allows us to interpret the distribution with respect to the geometry of the mainshock. If the reference focal mechanism is changed, the axes of rotation also change leading to a different distribution of angles. We tested alternative reference tensors derived from weighted and normalized Kostrov summations of the aftershocks [*Kostrov*, 1974; *Bailey et al*., 2010] and find similar results.

[10] Figure 2a shows the histogram of rotation angles for the double-couple mechanisms of events within 20 days of the Landers mainshock in region A, along with the probability density function (dashed black line) for randomly oriented double couples [*Kagan*, 1992]. Figure 2b presents corresponding results for all events in region A with $M \geq 2.2$, which provide a reference expectation for the background seismicity in the examined area. There are 412 events in the 20 day window and 1074 events that occurred in this region between the mainshock and the end of the catalog. The mean rotation angle, $\overline{\Omega}$, is 65° for the 20 day window and 61° for the long term data. Additionally, the histogram for the 20 day event window shows a greater percentage of rotation angles above 70° than the histogram for the long-term window. This suggests that early aftershocks in this region have focal mechanisms less aligned with the mainshock than the background seismicity in the region. To further quantify the extent of the differences between these two histograms, we use a two-sample Mann-Whitney *U* test [e.g., *Hollander and Wolfe*, 1973] to assess whether one of two independent samples has larger values than the other. When conducting this test, we first remove from the long-term set the events of the 20 day set. The *p*-value for the *U* test is 10^{-5} and nearly any confidence level chosen will lead to a rejection of the null hypothesis that the two samples are from the same population. Some of the aftershocks in region A are in a zone with east-west orientation (Figure 1) that has a high angle to most of the other seismicity. To test that the scatter in the rotation angles for the short-term data relative to the long-term events is not strongly influenced by the seismicity in this east-west branch, we remove those events and repeat the above statistical tests. The results indicate that the same behavior is observed with these events removed.

[11] Using the same procedure for the central portion of the Landers area (region B of Figure 1), we have 1384 events in the long-term set and 349 events in the short-term set (Figure 3). The histograms appear visually similar, suggesting that the focal mechanisms of early aftershocks here are produced in no different proportions than the background events. The mean rotation angle for events in region B is 50.6° over the 20 day window and 49.2° over the long term. The *U* test for these data sets yields a *p*-value of 0.37, from which we conclude that there is no statistical evidence that one sample has larger values than the other. Performing similar analyses for events in the southern portion (region C) of the Landers rupture, we find that the mean rotation angle in the short term is 51.3° and 48.7° over the long term (Figure 4). The *p*-value for the *U* test in this region is 0.03, which suggests that the early aftershocks have statistically larger rotation angles than the background seismicity, as with the other edge region.

[12] It is useful to examine the magnitude range over which the results remain statistically significant. For region A, the *p*-values are statistically significant at the 95% confidence level or greater for minimum magnitude $M_{\min}$ in the range $M_{\min} = 2.2$–2.7. Above $M_{\min} = 2.7$, the number of events in each sample is relatively small and, as a result, the statistical tests are no longer sensitive enough to resolve these effects. Region C is statistically significant at the 95% confidence level or greater for $M_{\min} = 2.2$–2.6, while region B is found not to be statistically significant at the 95% confidence level for any minimum magnitude.

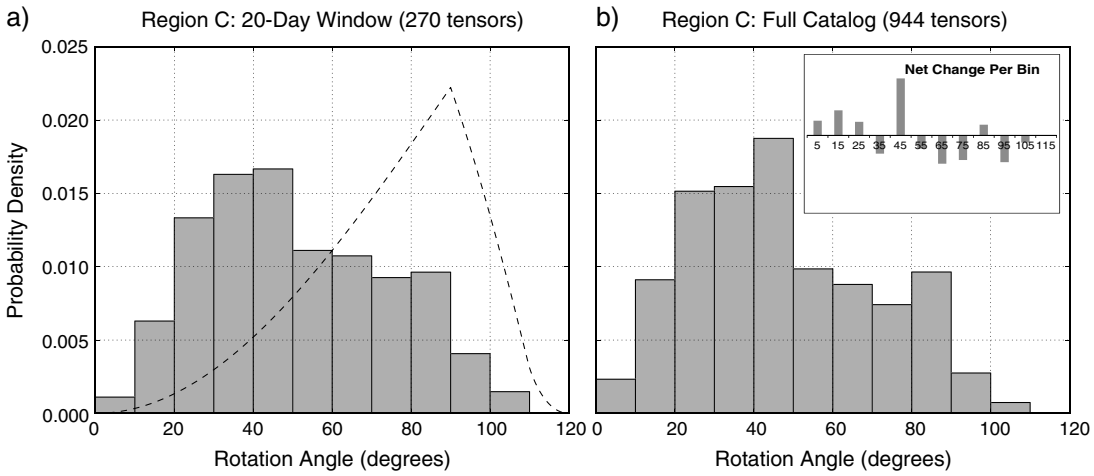

Figure 4. (a–b) Similar to Figure 2 for events in the southern region C of Figure 1. The results exhibit intermediate scatter and temporal evolution compared to the results for regions A and B. The inset in Figure 4b shows the angles mostly decrease from Figures 4a to 4b above 55°.

[13] The results of Figures 2–4 exhibit spatio-temporal variations in focal mechanism orientations. To obtain additional information on temporal evolution of these distributions in each region, we take first focal mechanisms within 5 days of the mainshock and compute the corresponding sets of rotation angles. This provides roughly 150–200 focal mechanisms for each region. Then we iteratively increase the time window duration while keeping the starting time (mainshock occurrence) fixed. For each window, we compute $\overline{\Omega}$ and continue this process until four years after the mainshock (28 June 1996). This procedure employs progressively larger number of events that provide increasingly more stable results that approach gradually (Figure 5) the long-term values in each of the three regions. In each region, $\overline{\Omega}$ decreases with time and stabilizes after a certain amount of time at the long-term values of Figures 2b, 3b, and 4b. The long-term mean values provide a measurement of how much the average focal mechanism deviates from the mainshock source configuration in a given space region. Because these values are obtained using time windows of 4 years, they should include some events that are not aftershocks. The mean rotation angles generally decrease monotonically in time, other than for a single data point in region C at 10 days after the mainshock. This suggests that as time increases new events are produced with focal mechanisms that relate more closely to the Landers mainshock than the earlier aftershocks. Region A has the longest temporal decay and requires 1–2 years to stabilize. The central region B has the fastest decay and takes only about six months to stabilize at the long-term value. The mean rotation angle for region B appears to decay with time like the other two areas, although this change is not detectable with the statistics used in the context of Figure 3. As with the northern edge, region C has a longer decay than the central section and takes over one year to stabilize at the long-term value.

[14] An alternative method of analyzing the rotation angles over time involves using a fixed number of events in the averaging window instead of an increasing amount of time. Using this type of sampling with various numbers of events per window produces the overall features of Figure 5, superposed with temporal oscillations that depend on the number of used events. A detailed analysis of the temporal oscillations requires careful analysis of various potential artifacts and is left for future work.

3. Fault Plane Solution Uncertainties

[15] There is a difference of approximately 4° between the mean rotation angle measured 5 days after the mainshock and the mean angle for the long-term seismicity in region A (Figure 2). The elevated mean rotation angles in the 20 day window relative to the background seismicity, and longer decay time to the background values near the main

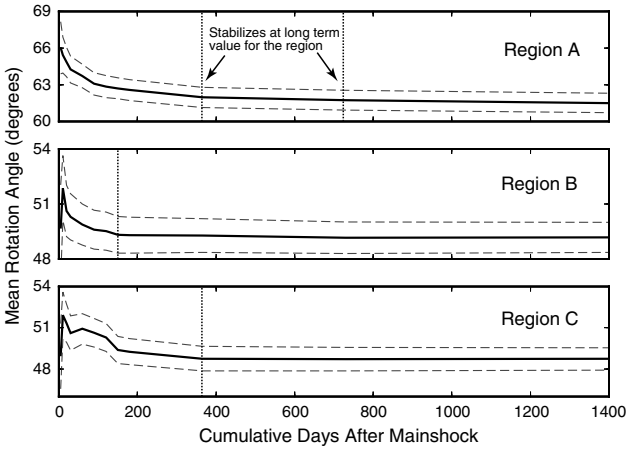

Figure 5. The mean rotation angles (solid lines) and 1-standard deviation bounds (dashed lines) as a function of time for the double-couple–constrained mechanisms of aftershocks in the three regions of Figure 1. All rotation angles are computed with respect to the Landers mainshock focal mechanism. The horizontal axis denotes the length of the employed cumulative time window after the mainshock. The time scale for the mean rotation angles to stabilize in the two edges regions A and C is over one year, whereas for the central region B it is about six months.

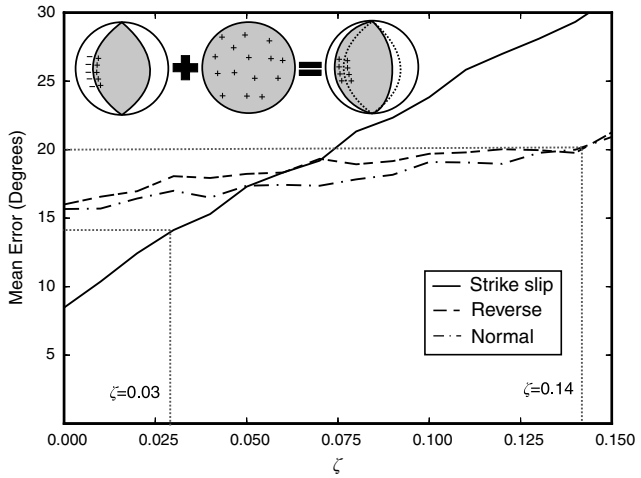

Figure 6. The uncertainty produced with the HASH algorithm by forcing a source with double-couple and isotropic components to be purely double-couple. The beach balls on top illustrate schematically how a small isotropic component can flip the polarities at stations near the nodal planes, leading to a rotation (error) in estimating a double-couple mechanism. The values shown correspond to an input range for the isotropic parameter ζ (equation (5)) in the range 0–0.15. The thick lines show how the inversion errors (in degrees) increase with ζ for the three basic double-couple mechanisms. The results indicate that the mean error of 4° observed in the focal mechanism catalog (Figures 2–4) may reflect neglected isotropic components of 0.03–0.15.

rupture ends (Figure 5) are statistically robust results. The set of faults associated with the Landers aftershocks have highly complex geometry and are prime settings for the production of rock damage during failure. Because the focal mechanism catalog of *Yang et al*. [2012] was derived with the constraint that each event is a pure double-couple, an isotropic component in the true source mechanism will lead to an error in the fault plane solution. Because isotropic radiation adds a constant value to every point on the focal sphere, some P wave radiation pattern values near the nodal planes may end up having their sign flipped relative to what is expected for a pure double-couple (Figure 6, inset). This can produce a large error in the double-couple–constrained solution. Below we test how significant such errors can be in the HASH algorithm by using synthetic first motion polarities.

[16] We represent the geometry of an earthquake source mechanism with a unit potency tensor $\hat{P}_{ij}$ [e.g., *Ben-Zion*, 2008]. The far-field P wave radiation pattern of a general $\hat{P}_{ij}$ can be written [e.g., *Pujol and Herrmann*, 1990; *Aki and Richards*, 2002] as

$$R^{\mathrm{P}} = \left(\sqrt{2}\gamma_i \hat{P}_{ij}\gamma_j\right) \tag{4}$$

where γ_i are elements of the direction cosine vector. A general earthquake source tensor can be decomposed into isotropic and deviatoric components, with the deviatoric part having a double-couple term and a remainder term (e.g., compensated linear vector dipole, referred to as CLVD). Given our focus on isotropic radiation, we assume that the deviatoric component is a pure DC and write $\hat{P}_{ij}$ as [*Zhu and Ben-Zion*, 2013]

$$\hat{P}_{ij} = \sqrt{1-\zeta^2}\hat{P}_{ij}^{\mathrm{DC}} + \zeta\hat{P}_{ij}^{\mathrm{I}} \tag{5}$$

[17] Here $\hat{P}_{ij}^{\mathrm{I}} = \sqrt{\frac{1}{3}}\delta_{ij}$ with δ_{ij} being the identity matrix, ζ is the fraction of the isotropic part of the source tensor taking values from -1 to 1 to account for both implosive and explosive cases, and $\hat{P}_{ij}^{\mathrm{DC}}$ is the potency tensor for an arbitrarily oriented double-couple. Using (4), the P wave radiation pattern for the double-couple component of $\hat{P}_{ij}$ can be written as

$$\sqrt{1-\zeta^2}\left(\sqrt{2}\gamma_i\hat{P}_{ij}^{\mathrm{DC}}\gamma_j\right) = \sqrt{1-\zeta^2}R_{\mathrm{DC}}^{\mathrm{P}} \tag{6}$$

where $R_{\mathrm{DC}}^{\mathrm{P}}$ is the P wave radiation pattern for an arbitrarily oriented double-couple [*Aki and Richards*, 2002] varying from -1 to 1. Similarly, the P wave radiation pattern for the isotropic component of $\hat{P}_{ij}$ can be written as

$$\zeta\sqrt{2}\gamma_i\hat{P}_{ij}^{\mathrm{I}}\gamma_j = \sqrt{\frac{2}{3}}\zeta\gamma_i\delta_{ij}\gamma_j = \sqrt{\frac{2}{3}}\zeta. \tag{7}$$

[18] We define an effective radiation pattern $\overline{R}^{\mathrm{P}}$ for a source mechanism that includes a fraction ζ of isotropic component as

$$\overline{R}^{\mathrm{P}} \equiv \left[R_{\mathrm{DC}}^{\mathrm{P}}\sqrt{1-\zeta^2} + \sqrt{\frac{2}{3}}\zeta\right] \tag{8}$$

[19] Along the double-couple nodal planes, where values are close to zero, a nonzero value of ζ can produce a shift of the actual nodal planes in the observed waveforms. Because grid search algorithms that use polarities expect each quadrant in the focal sphere to have the same size, any flipped polarities introduced by an isotropic component will lead to error in the derived fault plane solutions and cause a rotation in the obtained eigenvectors. To obtain quantitative estimates, we write $R_{\mathrm{DC}}^{\mathrm{P}}$ as a function of takeoff angle and azimuth as in equation (4.89) of *Aki and Richards* [2002], and use Monte Carlo simulations in two test cases to generate sets of radiation patterns for given ζ values. In the first case, we select 30 takeoff angles drawn from a uniform distribution over [0,90°] and 30 azimuths from a uniform distribution on [0,360°]. These are used to determine the radiation pattern for a specified strike, dip, and rake of the double-couple component; the particular sample size of 30 is an attempt to account for finite sampling of the focal sphere during any event. We then use the sign of the radiation pattern, along with the takeoff angles and azimuths, to determine the fault plane solution with HASH. This process is repeated 2000 times to get a set of fault plane solutions indicative of the range possible by the grid search algorithm.

[20] The assumed fault plane geometry of each event is used as a reference for computation of rotation angles with the solutions obtained from HASH. If this is done initially with $\zeta = 0$, the mean rotation angle, $\overline{\Omega}_0$, represents the total uncertainty in

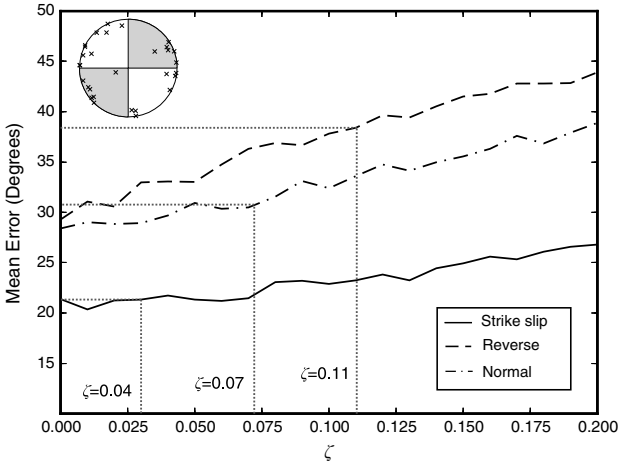

Figure 7. The uncertainty produced with the HASH algorithm for various levels of isotropic radiation using a ring-like station configuration with a sample realization illustrated by the focal sphere on top. The normal and reverse mechanisms are more sensitive than strike slip to the station configuration because more of their nodal regions are sampled with these source orientations. The estimated isotropic components for the three mechanisms are 0.04 for reverse, 0.07 for normal, and 0.11 for strike slip.

the algorithm itself with 30 stations used. The $\overline{\Omega}_0$ value can be used to estimate the added uncertainty, $\Delta\Omega_\zeta$, to a fault plane solution for a given value of ζ

$$\Delta\Omega_\zeta = \overline{\Omega}_\zeta - \overline{\Omega}_0 \tag{9}$$

where $\overline{\Omega}_\zeta$ is the mean rotation angle for a given ζ. We investigated three basic focal mechanism cases to document how the HASH algorithm behaves. Figure 6 shows the obtained $\Delta\Omega_\zeta$ values for each focal mechanism case with assumed ζ ranging from 0 to 0.15. For the Landers mainshock, the difference between the short- (5 day) and long-term mean rotation angles is approximately 4°. If this difference is purely due to isotropic component of radiation, the early aftershocks have on the average $\zeta \sim 0.03$ assuming strike slip mechanisms and $\zeta \sim 0.14$–0.15 for the reverse and normal cases. Because the distribution of focal mechanisms in the Landers area (Figures 2–4) is very diverse, the average ζ value for this region as estimated by the above technique would likely fall somewhere in the range of 0.05–0.10. The focal mechanisms retrieved in the synthetic tests with $\zeta = 0.03$ have an increase of the mean inversion misfit by 3.14% compared to the focal mechanisms with $\zeta = 0$. Examining the DC-constrained mechanisms of *Yang et al.* [2012] for the Landers aftershocks, we find that the mean inversion misfit for the 20 day window is 3% higher than the misfit for the long-term window. This is in very good agreement with our synthetic results.

[21] The synthetic results leading to Figure 6 correspond to an ideal situation with a uniform coverage of the focal sphere. To estimate effects of isotropic radiation in a more typical observational setting, we consider a second test case with takeoff angles sampled from a distribution that is concentrated near the edge of the focal sphere. In this case we draw takeoff angles from a normal distribution with a mean of 90° and a standard deviation of 30°. This corresponds to a situation where the majority of stations are near the edge of the focal sphere (Figure 7, inset). As before, we perform sets of 2000 inversions for realizations associated with 30 stations each, and calculate the mean rotation angle for varying fractions of isotropic component. The inversion errors for different isotropic components are shown in Figure 7. Because the station configuration is significantly different from that of the first case, the estimates of isotropic components for a given rotation error in Figure 7 differ from those of Figure 6, but both test cases produce similar trends. The reverse and normal focal mechanisms are more sensitive to the edge of the focal sphere than strike slip mechanisms. Based on the observed difference in the mean rotation angles of the short- and long-term results for region A (Figures 2a and 2b), we estimate average isotropic components of 0.11, 0.07, and 0.04 for events with strike-slip, normal, and reverse mechanisms, respectively. These numbers are in the same range as those obtained with uniform focal sphere sampling.

4. Discussion

[22] A general faulting process, not limited to a preexisting planar surface, produces brittle rock damage associated with changes of elastic moduli within and around the failure zone [e.g., *Lockner et al.*, 1977; *Hamiel et al.*, 2004; *Stanchits et al.*, 2006]. Seismic source tensors in regions sustaining coseismic changes of elastic moduli can have non-negligible isotropic components [*Ben-Zion and Ampuero*, 2009]. This is expected especially in regions without preexisting through-going fault traces, near the rupture ends, and around fault sections with large geometrical complexity [*Castro and Ben-Zion*, 2013]. In sections 2 and 3 we examine rotation angles of double-couple–constrained focal mechanisms of the 1992 Landers aftershock sequence [*Yang et al.*, 2012]. The analysis aims to clarify spatio-temporal variations of earthquake source tensors and possible existence of volumetric strain changes in the source volumes. The examined mechanisms are derived with the HASH algorithm [*Hardebeck and Shearer*, 2002] as double-couples, so the isotropic components of individual source tensors are by default zero. Nevertheless, the population of the double-couple mechanisms can be used to assess likely variations of the coseismic strain fields, including volumetric components, at different locations.

[23] The Landers mainshock propagated primarily in the north-northwest direction through a complex set of faults in the eastern California shear zone [*Wald and Heaton*, 1994]. The curved geometry of the Landers rupture, which is especially prominent in the northern section, should lead to coseismic generation of rock damage. The rupture and arrest processes near the north and south mainshock edges should include significant volumetric components that are especially prominent in the main propagation direction [e.g., *Ben-Zion et al.*, 2012]. We thus expect significant generation of rock damage around the northern end of the Landers rupture (Figure 1, region A), relatively minor damage in the central section (Figure 1, region B) and intermediate damage near the southern rupture end (Figure 1, region C). These expectations are consistent with the results of Figures 2–5. The rotation angles of the double-couple mechanisms of the early aftershocks in region A are closer to the random distribution than in regions B and C; the difference

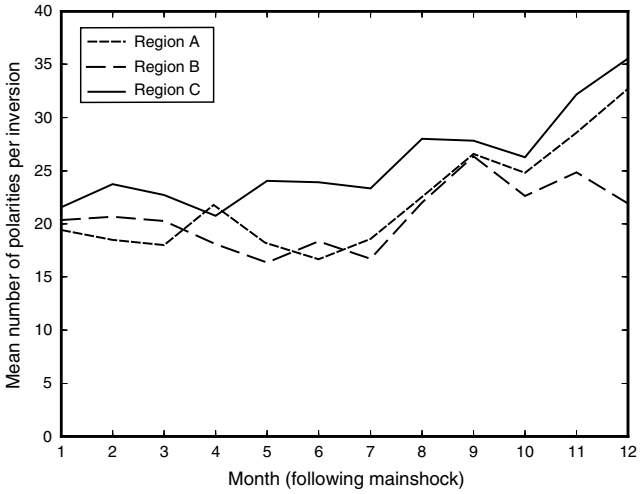

Figure 8. The mean number of polarities used for derivation of focal mechanisms in regions A–C of Figure 1 for each month following the Landers mainshock.

between the mean rotation angle of the early aftershocks and the long-term value is largest in the northern region A, intermediate in the southern region C, and smallest in the central region B; the same order characterizes the time scales for the mean rotation angle to stabilize at the long-term value.

[24] Numerous studies have pointed out that faulting on nonplanar geometries can produce deviatoric source tensors with CLVD components [e.g., *Julian et al*., 1998; *Bailey et al*., 2010]. In the present work we focus on isotropic source terms and show that deriving source tensors of earthquakes with small isotropic components (equations (5)–(8)) using an inversion algorithm that assumes purely double-couple mechanisms can lead to the observed variations in the rotation angles of the double-coupled–constrained mechanisms (Figures 6 and 7). We note that the analysis of section 3 intends to demonstrate effects associated with neglecting isotropic source term. These results do not imply that the observed variations in rotation angles are produced exclusively or predominantly by isotropic source components. A more complete analysis should examine the likely contributions to scatter in double-couple–constrained mechanisms of neglecting isotropic and CLVD components (along with other possible mechanisms). Such analysis requires additional methods not used in the present paper and is deferred to a future work.

[25] Our results indicate that aftershock focal mechanisms become more like the mainshock as time after the parent event increases. To verify that the observed pattern is not produced by a changing stations configuration, we examine (Figure 8) the mean number of polarities used in the grid search per event for each month following the mainshock. The results show very similar evolution for regions A and B where we observe the largest and smallest temporal variations. Moreover, for the first seven months the station coverage does not increase significantly and for two of the regions it even decreases slightly. As a significant portion of the temporal decay present in Figure 5 occurs during this time window, we conclude that the observed phenomena are not likely the result of an increase in station coverage. It could be possible that spatio-temporal migration of the examined events lead to progressive failures on different structures that contribute significantly to the observed changes in the rotation angle distributions. However, a plot of the aftershocks in the region color-coded by the occurrence day after the mainshock (see Figure S1 in the supporting information) does not show any systematic migration of earthquake epicenters.

[26] *Kagan* [2000] investigated temporal changes of rotation angle distributions between pairs of earthquakes in the Harvard CMT catalog with lapse times between event pairs from 0 to 120 days. In contrast to our results, *Kagan* [2000] found that the mean rotation angle increases slowly with time and interpreted this as indication that earthquakes occurring closer in time have more similar source processes than earthquakes occurring further apart. The different observed patterns may reflect different processes occurring at the different involved scales. Our study was designed specifically to analyze low magnitude aftershocks, covering small spatio-temporal scales that may reflect local processes within and around the mainshock rupture zone. The global study of *Kagan* [2000] with only $M > 5.5$ events likely average over the phenomena observed in this study. Furthermore, if the results of *Kagan* [2000] were to hold at the same scales of our study, the observed increase of the mean rotation angle immediately after the Landers mainshock may provide stronger evidence of a neglected isotropic component in the source region.

[27] When conducting the synthetic tests, we estimated the grid search uncertainty produced by neglecting ζ by shifting the total uncertainty for each value of ζ down with an amount equal to the mean rotation angle for $\zeta = 0$. This value is a measurement of the accuracy of the HASH grid search algorithm given the number of used stations, assumed station sampling over the focal sphere, and assumed focal mechanism. Subtracting this value is equivalent to linearizing the uncertainty as a function of ζ to estimate the added uncertainty for each value of ζ. For ζ values between 0 and 0.2, a linear approximation seems reasonable for all three basic focal mechanisms (Figures 6 and 7); a simple linear regression to these data yields R^2 values larger than 0.90. Although the linear trend may not continue beyond 0.20, we have only considered values below this threshold so the results provide adequate estimates of the uncertainty produced due to neglecting ζ in the grid search.

[28] The results of this study show that early aftershocks of the 1992 Landers earthquake have source mechanisms that are less aligned with the mainshock than the background seismicity occurring in the same region over multiple years. This could reflect, at least partly, a true phenomenon resulting from complex coseismic and early postseismic strain fields near the rupture ends. However, the variations in rotation angles of the double-couple–constrained mechanisms may also be produced, at least partially, as artifacts of the inversion process neglecting small isotropic source terms. These are expected to be generated by damage-related radiation [*Ben-Zion and Ampuero*, 2009] and other sources of volumetric deformation in fault sections with large geometrical complexity and near rupture ends [e.g., *Sibson*, 1986; *Ben-Zion et al*., 2012]. A more direct estimate of isotropic earthquake source terms, and their contribution to scatter in double-couple–constrained mechanisms, can be done by combining full derivation of earthquake source tensors with analysis of the type done here. This will be done in a future work.

[29] **Acknowledgments.** We thank Lupei Zhu and Iain Bailey for useful discussions. The study was supported by the Southern California Earthquake Center (based on NSF Cooperative Agreement EAR-0529922 and USGS Cooperative Agreement 07HQAC0026) and the National Science Foundation (grant EAR-0944198). The manuscript benefitted from constructive comments of two anonymous referees.

References

Aki, K., and P. G. Richards (2002), *Quantitative Seismology*, 2nd edn, University Science Books, Sausalito, CA, USA.

Ampuero, J.-P., and F. A. Dahlen (2005), Ambiguity of the moment tensor, *Bull. seismol. Soc. Am.*, *95*, 390–400.

Backus, G., and M. Mulcahy (1976), Moment Tensors and other Phenomenological Descriptions of Seismic Sources—I Continuous Displacements, *Geophys. J. R. Astron. Soc.*, *46*(2), 341–361.

Bailey, I. W., Y. Ben-Zion, T. W. Becker, and M. Holschneider (2010), Quantifying focal mechanism heterogeneity for fault zones in Southern and Central California, *Geophys. J. Int.*, *183*, 433–450, doi:10.1111/j.1365-246X.2010.04745.X.

Ben-Zion, Y. (2001), Dynamic ruptures in recent models of earthquake faults, *J. Mech. Phys. Solids.*, *49*(9), 2209–2244.

Ben-Zion, Y. (2003), Appendix 2, Key Formulas in Earthquake Seismology, in *International Handbook of Earthquake and Engineering Seismology*, editexd by W. H. K. Lee, H. Kanamori, P. C. Jennings, and C. Kisslinger, Part B, 1857–1875, Academic Press, London, UK.

Ben-Zion, Y. (2008), Collective Behavior of Earthquakes and Faults: Continuum-Discrete Transitions, Progressive Evolutionary Changes and Different Dynamic Regimes, *Rev. Geophys.*, *46*, RG4006, doi:10.1029/2008RG000260.

Ben-Zion, Y., and J. Ampuero (2009), Seismic radiation from regions sustaining material damage, *Geophys. J. Int.*, *178*(3), 1351–1356.

Ben-Zion, Y., and L. Zhu (2002), Potency-magnitude Scaling Relations for Southern California Earthquakes with $1.0 < ML < 7.0$, *Geophys. J. Int.*, *148*, F1–F5.

Ben-Zion, Y., T. Rockwell, Z. Shi, and S. Xu (2012), Reversed-polarity secondary deformation structures near fault stepovers, *J. Appl. Mech.*, *79*, 031025, doi:10.1115/1.4006154.

Brune, J., S. Brown, and P. Johnson (1993), Rupture mechanism and interface separation in foam rubber models of earthquakes: a possible solution to the heat flow paradox and the paradox of large overthrusts, *Tectonophysics*, *218*, 59–67.

Castro, R. R., and Y. Ben-Zion (2013), Potential Signatures of Damage-Related Radiation from Aftershocks of the 4 April 2010 (Mw 7.2) El Mayor-Cucapah Earthquake, Baja California, México, *Bull. Seismol, Soc. Am.*, *103*, doi:10.1785/0120120163.

Chapman, C., and W. Leaney (2012), A new moment-tensor decomposition for seismic events in anisotropic media, *Geophys. J. Int.*, *188*(1), 343–370.

Dufumier, H., and L. Rivera (1997), On the resolution of the isotropic component in moment tensor inversion, *Geophys. J. Int.*, *131*(3), 595–606.

Eshelby, J. (1957), The Determination of the Elastic Field of an Ellipsoidal Inclusion, and Related Problems, *Proc. R. Soc. London. A.*, *241*(1226), 376–396.

Hamiel, Y., Y. Liu, V. Lyakhovsky, Y. Ben-Zion, and D. Lockner (2004), A Visco-Elastic Damage Model with Applications to Stable and Unstable fracturing, *Geophys. J. Int.*, *159*, 1155–1165, doi:10.1111/j.1365-246X.2004.02452.X.

Hardebeck, J., and P. Shearer (2002), A new method for determining first-motion focal mechanisms, *Bull. Seismol. Soc. Am.*, *92*(6), 2264—2276.

Hollander, M., and D. Wolfe 1973, *Nonparametric Statistical Methods*, John Wiley & Sons, Inc, New York, New York, USA.

Julian, B., A.D. Miller, and G.R. Foulger (1998), Non-Double-Couple Earthquakes 1. Theory, *Rev. Geophys.*, *36*(4), 525–549.

Kagan, Y. (1991), 3-D rotation of double-couple earthquake sources, *Geophys. J. Int.*, *106*(3), 709–716.

Kagan, Y. (1992), Correlations of earthquake focal mechanisms, *Geophys. J. Int.*, *110*(2), 305–320.

Kagan, Y. (2000), Temporal correlations of earthquake focal mechanisms, *Geophys. J. Int.*, *143*, 881–897.

Kostrov, V. V. (1974), Seismic moment and energy of earthquakes, and seismic flow of rock, *Earth Phys.*, *1*, 23–40.

Kuipers, J. (2002), *Quaternions and Rotations: a Primer with Applications to Orbits, Aerospace, and Virtual Reality*, Princeton University Press, Princeton, NJ, USA.

Lockner, D., J. Walsh, and J. Byerlee (1977), Changes in Seismic Velocity and Attenuation During Deformation of Granite, *J. Geophys. Res.*, *82*, 5374–5378.

Pujol, J., and R. Herrmann (1990), A student's guide to point sources in homogeneous media, *Seismol. Res. Lett.*, *61*(3–4), 209–221.

Reid, H. F. (1910), The mechanics of the earthquake, in *The California Earthquake of April 18, 1906*, Vol. *2*, Carnegie Institute, Washington, DC, USA.

Rice, J. R. (2006), Heating and weakening of faults during earthquake slip, *J. Geophys. Res.*, *111*, B05311, doi:10.1029/2005JB004006.

Riedesel, M., and T. Jordan (1989), Display and assessment of seismic moment tensors, *Bull. Seismol. Soc. Am.*, *79*(1), 85–100.

Sibson, R. H. (1986), Rupture interactions with fault jogs, *Earthquake Source Mechanics*, *37*, Geophys. Monogr. Ser., edited by S. Das, J. Boatwright, and C. H. Scholz, pp. 157–167, AGU, Washington, DC.

Stanchits, S., S. Vinciguerra, and G. Dresen (2006), Ultrasonic velocities, acoustic emission characteristics and crack damage of basalt and granite, *Pure Appl. Geophys.*, *163*, 975–994.

Wald, D., and T. Heaton (1994), Spatial and temporal distribution of slip for the 1992 Landers, California, earthquake, *Bull. Seismol. Soc. Am.*, *84*, 668–691.

Yang, W., E. Hauksson, and P. Shearer (2012), Computing a Large Refined Catalog of Focal Mechanisms for Southern California (1981–2010): Temporal Stability of the Style of Faulting, *Bull. Seismol. Soc. Am.*, *102*(3), 1179–1194.

Zhu, L., and Y. Ben-Zion (2013), Parameterization of general seismic potency and moment tensors for source inversion of seismic waveform data, *Geophys. J. Int.*, in press, doi:10.1093/gji/ggt137.